REPORT

SURFACE CHEMISTRY

Low-temperature activation of methane on the IrO_2(110) surface

Zhu Liang,[1] Tao Li,[1] Minkyu Kim,[2] Aravind Asthagiri,[2] Jason F. Weaver[1]*

Methane undergoes highly facile C–H bond cleavage on the stoichiometric IrO_2(110) surface. From temperature-programmed reaction spectroscopy experiments, we found that methane molecularly adsorbed as a strongly bound σ complex on IrO_2(110) and that a large fraction of the adsorbed complexes underwent C–H bond cleavage at temperatures as low as 150 kelvin (K). The initial dissociation probability of methane on IrO_2(110) decreased from 80 to 20% with increasing surface temperature from 175 to 300 K. We estimate that the activation energy for methane C–H bond cleavage is 9.5 kilojoule per mole (kJ/mol) lower than the binding energy of the adsorbed precursor on IrO_2(110), and equal to a value of ~28.5 kJ/mol. Low-temperature activation may avoid unwanted side reactions in the development of catalytic processes to selectively convert methane to value-added products.

The increasing supply of natural gas provides substantial motivation for developing catalytic processes that can efficiently and directly transform methane (CH_4) to value-added products such as methanol, formaldehyde, or ethylene. Selective catalytic transformations of CH_4 remain a major challenge in catalysis (*1*, *2*). A limitation with most existing heterogeneous catalysts is that initial C–H bond cleavage is rate controlling (*1*), so subsequent reaction steps occur rapidly and are difficult to control. Achieving CH_4 activation at low temperature could eliminate this limitation and allow for its selective oxidation. However, catalytic materials that can readily activate CH_4 at low temperatures (e.g., below 300 K) have not been reported.

The activation of light alkanes on solid surfaces can occur by direct and precursor-mediated mechanisms (*3*). In the direct mechanism, the alkane molecule undergoes C–H bond cleavage during its initial collision with the surface, and reaction is activated with respect to the gas-phase energy level. In the precursor-mediated mechanism, the alkane first adsorbs intact on the surface, and the resulting molecularly adsorbed state serves as a precursor for C–H bond cleavage. Dissociation by the precursor-mediated mechanism is facile when the activation energy for C–H bond cleavage (E_r) is smaller than the activation energy for desorption (E_d) of the molecularly adsorbed precursor. Molecular beam experiments show that CH_4 dissociation is activated ($E_r > E_d$) on the many crystalline transition-metal surfaces that have been investigated (*3*). Facile dissociation ($E_r < E_d$) of CH_4 on a solid surface has not been previously reported, but other light alkanes do undergo facile activation on certain facets of metallic Ir and Pt (*4*–*7*). Prior studies also report only weak molecular adsorption of alkanes on many metal oxides, including alkaline-earth oxides, rare-earth oxides, and TiO_2 (*8*–*10*).

We have reported that specific facets of late transition-metal oxides, in particular PdO(101), can promote alkane C–H bond cleavage (*11*, *12*). The key aspect of these surfaces is the presence of pairs of coordinatively unsaturated (cus) metal and oxygen atoms on the surface that promote the formation and facile C–H bond cleavage of adsorbed alkane σ complexes (*11*). We have shown that the cus-Pd sites of PdO(101) datively bond with alkanes (*11*–*13*) and that the resulting molecularly adsorbed species are analogous to coordination compounds known as alkane σ complexes (*14*). The dative interaction with cus-metal sites facilitates alkane activation by both strengthening the alkane-surface binding as well as weakening the Pd-coordinated C–H bonds. The cus-oxygen atoms also play a central role in alkane C–H bond cleavage on PdO(101) by acting as H-atom acceptors. In situ measurements show that formation of a PdO(101) layer gives rise to high rates of CH_4 oxidation over Pd surfaces under steady-state conditions at elevated pressure, thus demonstrating that fundamental studies with PdO(101) are directly relevant for understanding CH_4 oxidation over Pd surfaces under realistic conditions (*15*).

Density functional theory (DFT) calculations predict that small alkanes also form strongly bound σ complexes on rutile RuO_2 and IrO_2 surfaces (*11*, *16*–*20*). We have experimentally confirmed the formation of alkane σ complexes on RuO_2(110) and also shown that *n*-butane undergoes facile C–H bond cleavage during temperature-programmed reaction spectroscopy (TPRS) experiments in ultrahigh vacuum (UHV) (*19*, *20*). Dispersion-corrected DFT calculations predict that the binding energy of the CH_4 σ complex on IrO_2(110) is greater by about 40 kJ/mol than the energy barrier for C–H bond cleavage, so that CH_4 activation should occur at high rates on IrO_2(110) at temperatures as low as 100 K (*17*, *18*).

The facile activation of CH_4 by the IrO_2(110) surface reinforces earlier studies that show an unusual ability of iridium to activate hydrocarbon C–H bonds. As originally reported by Ardntsen and Bergman (*21*), cationic Ir(III) complexes are among the most highly reactive transition-metal compounds known for promoting C–H bond activation. Further, crystalline surfaces of metallic Ir exhibit the highest activity toward alkane C–H bond cleavage among the metal surfaces that have been investigated (*3*), and the presence of low-coordination surface sites strongly enhances the reactivity of Ir and other metals toward alkane activation (*4*, *6*, *7*, *22*). A common feature among these systems is the availability of coordinatively unsaturated Ir centers to bind and activate adsorbed alkanes.

Experimental reports of the growth and surface chemistry of crystalline IrO_2 are sparse because well-defined IrO_2 surfaces are challenging to prepare for fundamental UHV studies. At the O_2 partial pressures typically used in UHV experiments, oxygen adsorption on crystalline Ir surfaces reaches an effective saturation at submonolayer O-atom coverages [~0.50 monolayer (ML)] because kinetic limitations suppress more-extensive oxygen uptake. An in situ surface x-ray diffraction study shows that relatively thick layers of rutile IrO_2, exposing (110) and (100) facets, can form during Ir(111) oxidation but only when the O_2 partial pressure and temperature are >100 mbar and 775 K (*23*). Oxidation of Ir(111) with plasma-generated oxygen beams can produce multilayer IrO_2 structures under UHV conditions (*24*, *25*). Rai *et al.* reported that a high-quality IrO_2(100) layer forms during Ir(111) oxidation with gaseous O atoms, with the oxide saturating at a thickness of about four layers for growth temperatures below ~650 K (*25*). However, the IrO_2(100) layer was completely oxygen terminated, so this surface would be chemically inactive for CH_4 reactions at moderate temperature. Thus, the formation of relatively thick, rutile IrO_2(110) surfaces via metallic Ir oxidation that expose cus-Ir sites occurs only at sufficiently high temperature and requires relatively high-oxidant fluxes.

We investigated the adsorption and C–H bond activation of CH_4 on a high-quality IrO_2(110) layer that was grown by oxidizing Ir(100) at 775 K and an O_2 partial pressure of 5 torr. We found that CH_4 readily undergoes C–H bond cleavage on the IrO_2(110) surface at temperatures down to at least 150 K. Analysis of temperature-dependent rate data shows that the initial dissociation of CH_4 on IrO_2(110) occurs through a precursor-mediated process wherein the activation energy for initial C–H bond cleavage is 9.5 kJ/mol lower than the binding energy of the molecularly adsorbed precursor.

The stoichiometric termination of rutile IrO_2(110) has a rectangular unit cell with dimensions of (3.16 Å by 6.36 Å) with the corresponding lattice vectors aligned along the [001] and [$\bar{1}$10] crystallographic directions, respectively (Fig. 1A).

[1]Department of Chemical Engineering, University of Florida, Gainesville, FL 32611, USA. [2]William G. Lowrie Chemical and Biomolecular Engineering, The Ohio State University, Columbus, OH 43210, USA.
*Corresponding author. Email: weaver@che.ufl.edu

Rows of cus-Ir atoms (Ir_{cus}) are separated by rows of bridging O atoms (O_{br}) that run parallel to the [001] direction. The Ir_{cus} and O_{br} atoms each lack a bonding partner compared with the bulk and expose single coordination vacancies. On the basis of the IrO_2(110) unit cell, the areal densities of Ir_{cus} atoms and O_{br} atoms would each be equal to 37% of the surface-atom density of Ir(100). Because the cus-metal atoms are active adsorption sites, we specify adsorbate coverages in units of monolayer, where 1 ML is equal to the density of Ir_{cus} atoms on the IrO_2(110) surface.

Oxidation of Ir(100) at 775 K and an O_2 partial pressure of 5 torr produced a high-quality IrO_2(110) layer that exposed the stoichiometric termination. We describe our experimental methods in the supplementary materials. A representative low-energy electron diffraction (LEED) pattern obtained after oxidizing Ir(100) to form the IrO_2(110) layer (Fig. 1B) agreed quantitatively with that simulated for two rotational domains of the IrO_2(110) structure with unit-cell dimensions of 3.16 Å by 6.36 Å. The IrO_2(110) lattice vectors align with the high-symmetry [001] and [010] directions of the Ir(100) growth substrate. The absence of Ir(100) diffraction spots in the LEED pattern is consistent with the presence of a conformal IrO_2(110) layer that is thick enough to completely attenuate the elastic scattering of electrons from the underlying Ir(100) substrate. The IrO_2(110) layer is stable to a temperature of ~725 K but thermally decomposes at higher temperature. Quantification of the O_2 temperature-programmed desorption (TPD) feature centered at ~900 K (fig. S1) allows us to estimate that the IrO_2(110) film contained 46 ML of O atoms and was ~3.5 nm thick. We confirmed that the IrO_2(110) layer was stoichiometrically terminated by using TPRS to characterize the adsorption behavior of O_2 and H_2O (fig. S2).

The TPRS traces obtained after adsorbing low and high CH_4 coverages (0.10 and 0.53 ML; Fig. 2, A and B) on the IrO_2(110) surface at 88 K revealed that a large fraction of the adsorbed CH_4 oxidizes to CO, CO_2, and H_2O during heating, with the CO and CO_2 products desorbing between ~400 and 600 K. The small CO TPRS feature near 250 K is consistent with a small quantity of CO that adsorbed from the vacuum background. The H_2O TPRS feature is broader than the CO and CO_2 features and spanned a range from ~400 to 750 K. Desorption of CH_4 also occurred with separate TPRS peaks centered at ~130 and 515 K. The low-temperature TPRS peak is characteristic of the desorption of a CH_4 σ complex that is bound strongly to the IrO_2(110) surface (~34 to 43 kJ/mol). In contrast, Redhead analysis of the high-temperature CH_4 peak suggests an activation energy for desorption (130 to 140 kJ/mol) that is far too high for this TPRS peak to originate from molecularly adsorbed CH_4. We confirmed that the high-temperature CH_4 peak results from the recombination of adsorbed CH_3 groups and H atoms by performing experiments of CD_4 adsorption onto an as-prepared IrO_2(110) film that was covered by a small amount of residual H atoms (see supplementary materials). On the basis of the detected mass fragments, these measurements demonstrate that only CD_4 desorbs in the TPRS peak at 130 K, whereas both CD_4 and CD_3H contribute to the TPRS peak near 515 K (fig. S3). Below, we show that energies derived from DFT calculations also support our assignments of the low- and high-temperature CH_4 TPRS peaks to molecular versus recombinative desorption processes.

The TPRS data demonstrate that a large quantity of CH_4 undergoes C–H bond activation on the IrO_2(110) surface, with the dissociated products oxidizing to CO, CO_2, and H_2O and also recombining to CH_4 at higher temperature. The observed reactivity is consistent with a precursor-mediated mechanism wherein a fraction of the adsorbed CH_4 σ complexes undergo C–H bond cleavage rather than desorbing, and the resulting CH_3 and OH fragments react during continued heating. An implication is that CH_4 C–H bond cleavage occurred readily on IrO_2(110) at temperatures as low as ~150 K and even lower, i.e., below the temperatures at which the adsorbed complexes desorb during TPRS. We are unaware of other materials that exhibit such high activity toward promoting CH_4 C–H bond cleavage.

The TPRS yields of reacted versus unreacted CH_4 on IrO_2(110) as a function of the CH_4 exposure performed at 88 K are shown in Fig. 2C. We define the yield of reacted CH_4 as the sum of the yields of CO, CO_2, and CH_4 that desorbed in the TPRS peak at ~515 K, which we attribute to recombinatively desorbed CH_4, and the yield of unreacted CH_4 ("molecular") as equal to the amount of CH_4 that desorbed in the low-temperature TPRS peak. The yield of reacted CH_4 increased as the exposure initially increased, while the yield of unreacted CH_4 remained quite low. More than 85% of the adsorbed CH_4 reacted during TPRS at total CH_4 coverages below ~0.30 ML. The yield of reacted CH_4 plateaued at ~0.30 ML after ~0.44-ML exposure. The yield of unreacted CH_4 increased only after the yield of reacted CH_4 had nearly saturated, demonstrating that the IrO_2(110) surface is highly reactive toward CH_4 at CH_4 coverages below about 0.33 ML. The total CH_4 coverage saturated at a value near 0.53 ML. We have reported a similar saturation coverage of CH_4 on the RuO_2(110) surface at 80 K (*19*). Thus, ~55% of the adsorbed CH_4 on IrO_2(110) reacted during TPRS when the CH_4 layer was saturated. The large quantity of CH_4 that reacts during TPRS is consistent with C–H bond activation occurring on the Ir_{cus} and O_{br} sites that are present on the crystalline terraces of the IrO_2(110) surface.

The change in TPRS yields of reaction products with CH_4 exposure is shown in Fig. 2D. Dissociated CH_4 preferentially oxidized to CO, CO_2, and H_2O during TPRS for initial CH_4 coverages below ~0.16 ML, but the selectivity toward oxidation over recombination continuously decreased as the total reaction yield increased. The oxidized and recombined yields became equal at ~0.16 ML when the total reaction yield reached saturation at 0.30 ML. The CO_2 yield was ~1.4 times higher

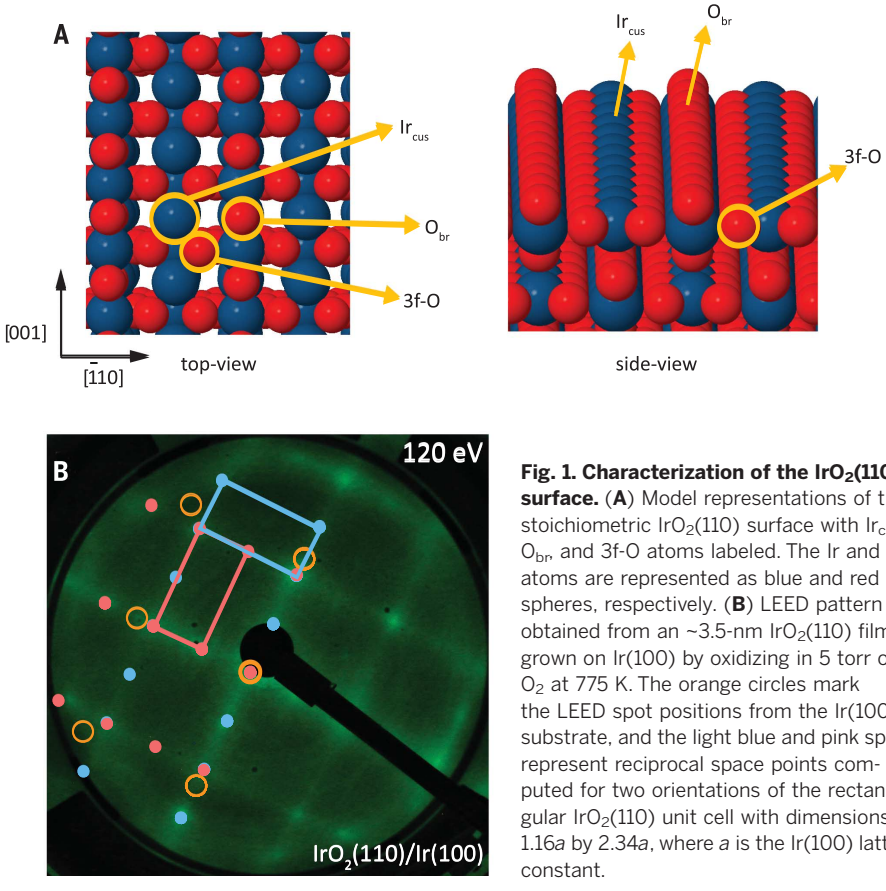

Fig. 1. Characterization of the IrO_2(110) surface. (**A**) Model representations of the stoichiometric IrO_2(110) surface with Ir_{cus}, O_{br}, and 3f-O atoms labeled. The Ir and O atoms are represented as blue and red spheres, respectively. (**B**) LEED pattern obtained from an ~3.5-nm IrO_2(110) film grown on Ir(100) by oxidizing in 5 torr of O_2 at 775 K. The orange circles mark the LEED spot positions from the Ir(100) substrate, and the light blue and pink spots represent reciprocal space points computed for two orientations of the rectangular IrO_2(110) unit cell with dimensions of 1.16*a* by 2.34*a*, where *a* is the Ir(100) lattice constant.

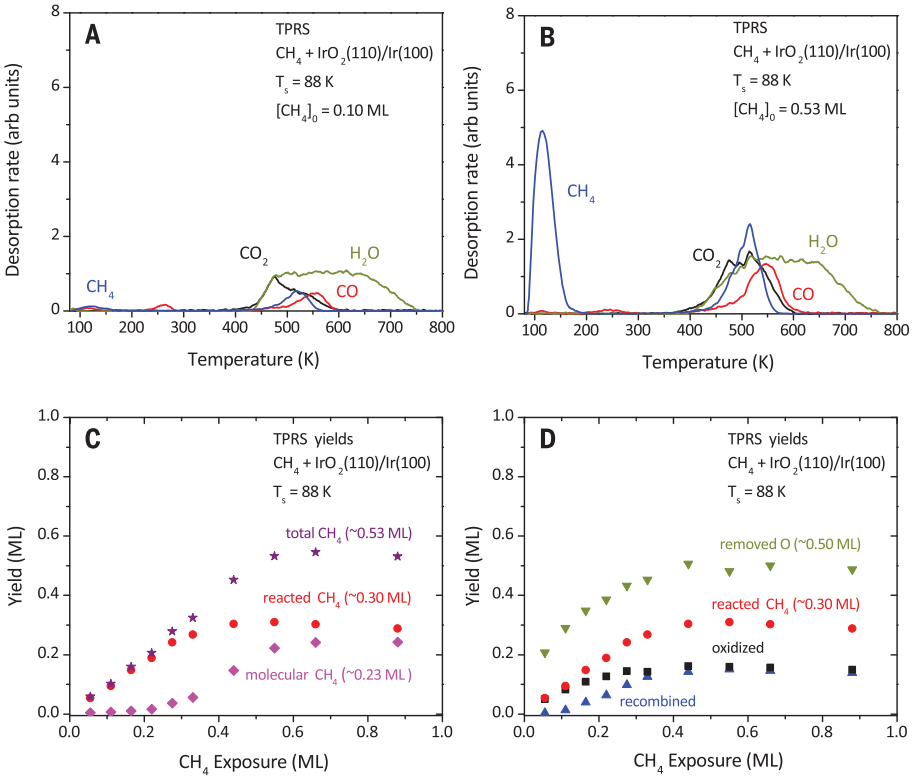

Fig. 2 Adsorption and reaction of CH_4 on $IrO_2(110)$. TPRS spectra of CH_4, H_2O, CO, and CO_2 obtained after adsorbing CH_4 on $IrO_2(110)$ at 88 K to generate initial CH_4 coverages of (**A**) 0.10 ML and (**B**) 0.53 ML. (**C**) TPRS yields of molecularly desorbed and reacted methane and the total CH_4 TPRS yield as a function of the CH_4 exposure to the surface. (**D**) Total yield of reacted CH_4, yields of oxidized CH_4 (CO + CO_2) and recombinatively desorbed CH_4, and the total amount of O atoms removed from the oxide during TPRS as a function of the CH_4 exposure.

than the CO yield at all CH_4 coverages, with yields reaching saturation values of 0.09 and 0.065 ML. Lastly, CH_4 oxidation during TPRS removed ~0.50 ML of O atoms from the $IrO_2(110)$ surface when the yield of oxidized products saturated, which is equal to half of the O_{br}-site concentration. We speculate that stoichiometric constraints as well as a relatively high stability of HO_{br} groups play an important role in determining the total reaction yield in addition to the branching between CH_4 oxidation and recombination during TPRS.

We evaluated experimental estimates of the CH_4 dissociation probability obtained as a function of the surface temperature using a kinetic model for the precursor-mediated dissociation of CH_4. The dissociation of an alkane from a molecularly adsorbed precursor state was represented by the following kinetic scheme (*3*, *6*)

$$\mathrm{RH(g)} \underset{k_d}{\overset{\xi F}{\rightleftharpoons}} \mathrm{RH(ad)} \xrightarrow{k_r} \mathrm{R(ad)} + \mathrm{H(ad)}$$

where RH represents an alkane molecule, ξ is the probability for molecular adsorption, F is the incident flux of gaseous RH at the surface, and k_d and k_r are rate coefficients for desorption and dissociation ("reaction") via C–H bond cleavage of the molecularly adsorbed RH σ complex. The kinetic scheme treats the reaction step as irreversible and is applicable at a temperature below that at which recombination becomes kinetically relevant. We assumed that the probability for CH_4 to adsorb molecularly into the σ-complex state is unity and independent of the surface temperature, because molecular adsorption is nonactivated and the impingent CH_4 molecules have kinetic energies that are much lower than the strength of the molecule-surface interaction (~2.5 versus 40 kJ/mol) (*3*). Molecular beam scattering experiments show that probabilities for nonactivated adsorption are nearly independent of the surface temperature (*26*). The following expression for the dissociative chemisorption probability in the limit of zero coverage (S_0) was derived by applying the steady-state approximation to the rate of formation of molecularly adsorbed alkanes:

$$S_0 = \frac{\xi k_r}{k_r + k_d}$$

If we assume that the Arrhenius equation describes the temperature dependence of each rate coefficient, then

$$\ln\left(\frac{\xi}{S_0} - 1\right) = \ln\left(\frac{\nu_d}{\nu_r}\right) - \frac{(E_d - E_r)}{RT_s}$$

where ν_j and E_j represent the prefactor and activation energy for reaction j, and T_s is the surface temperature. Thus, if CH_4 dissociates on $IrO_2(110)$ by a precursor-mediated mechanism, then a plot of $\ln(\frac{\xi}{S_0} - 1)$ versus $\frac{1}{T_s}$ will be linear and the Arrhenius construction will provide values for the apparent prefactor $\frac{\nu_r}{\nu_d}$ and activation energy $E_r - E_d$ for initial C–H bond cleavage.

To obtain estimates of the CH_4 dissociation probability, we measured the TPRS yields of reacted CH_4 (CO, CO_2, and recombinatively desorbed CH_4) as a function of the CH_4 exposure at several fixed surface temperatures between 175 and 300 K. We selected 175 K as the lower limit because this temperature lies above the trailing edge of the low-temperature CH_4 TPD peak. Because molecularly adsorbed CH_4 accumulates negligibly above 175 K, the TPRS yields of CO, CO_2, and recombinatively desorbed CH_4 were equal to the amount of CH_4 that dissociated on the surface during the CH_4 exposures. We selected 300 K as the upper limit to minimize the loss of surface oxygen via product desorption and thus avoid possible changes in surface reactivity that could occur during the CH_4 exposures caused by partial reduction of the oxide surface. Our TPRS results also showed that recombination of CH_3 and H atoms was negligible below 300 K and could be ignored in the analysis.

We measured CH_4 reaction yields as a function of the exposure at several T_s values; exposures were short to maintain low coverages of the reaction products. Each isotherm of the reaction yield versus exposure (Fig. 3A) was well approximated as linear, with the slopes decreasing with increasing T_s. The linear behavior was expected because the probability for dissociative chemisorption is approximately independent of the adsorbate coverage at low coverage. In this limit, the coverage of dissociated CH_4 [R] is given by the equation, $[R] = S_0 F t$ where the CH_4 exposure is equal to the product of the exposure time t and the incident flux F, which we estimated as 1.1×10^{-2} ML/s. The slope of the initial portion of an isotherm is thus equal to the initial dissociation probability of CH_4 on $IrO_2(110)$ for the T_s at which the exposure was conducted.

Our estimates of the initial dissociation probability S_0 of CH_4 on $IrO_2(110)$ at various T_s are plotted in Fig. 3B along with the curve that represents the expression S_0 (T_s) determined from our kinetic analysis, as discussed below. The initial dissociation probability decreased from about 80 to 19% with increasing T_s from 175 to 300 K. The $IrO_2(110)$ surface was markedly active toward promoting C–H bond cleavage: 80% of the CH_4 molecules that collide with the clean surface underwent C–H bond scission at a surface temperature of only 175 K. The decrease in initial dissociation probability with increasing T_s is characteristic of a facile precursor-mediated mechanism.

The excellent linear fit of $\ln(\frac{\xi}{S_0} - 1)$ versus $\frac{1}{T_s}$ (Fig. 3C) further supports the conclusion that CH_4 dissociation on $IrO_2(110)$ occurs by a precursor-mediated mechanism, with an apparent prefactor of 6.2×10^{-3} and an activation energy of –9.5 kJ/mol (negative relative to the gas-phase reference). The apparent activation energy and prefactor for reaction depend only weakly on the value of ξ

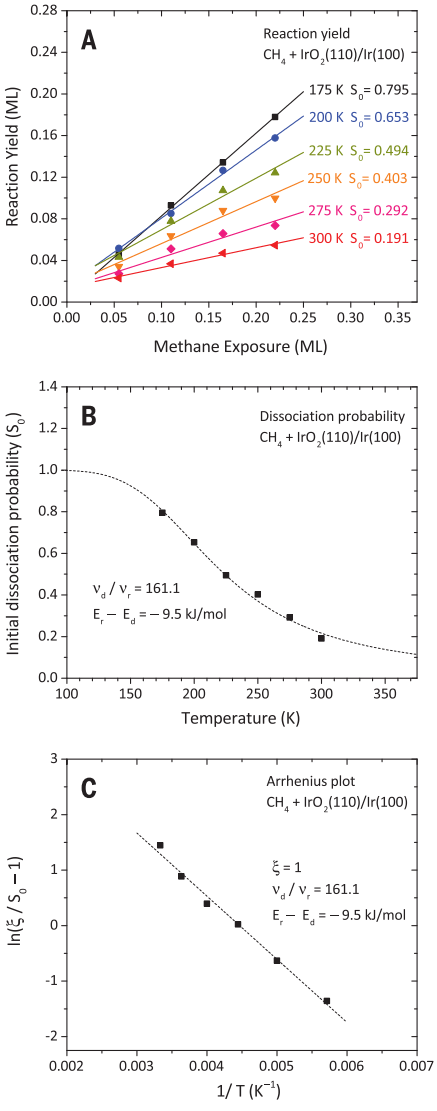

Fig. 3. Kinetic analysis of CH_4 dissociation on the IrO_2(110) surface. (**A**) Reaction yield versus CH_4 exposure to IrO_2(110) for different surface temperatures. (**B**) Initial dissociation probability versus surface temperature and (**C**) Arrhenius plot as discussed in the text.

used in the analysis. Our analysis of the low-temperature CH_4 TPRS peak suggests a binding energy of ~38 kJ/mol at low CH_4 coverage, from which we estimate a value of 28.5 kJ/mol for the activation energy of C–H bond cleavage of the CH_4 σ complex on IrO_2(110). For comparison, the reaction barrier that we estimate for CH_4 activation on IrO_2(110) is roughly half of that for CH_4 activation on PdO(101) (28.5 versus 56 kJ/mol).

The energy diagrams that we computed for the formation and dissociation of a CH_4 σ complex on IrO_2(110) as well as images of the initial, transition, and final states are shown in Fig. 4. The energies were determined with conventional DFT and the dispersion-corrected DFT-D3 method (*27*), both of which use the Perdew-Burke-Ernzerhof (PBE) exchange-correlation functional. Details of

Fig. 4. Energy diagrams for the formation and C–H bond cleavage of a CH_4 σ complex on IrO_2(110). Shown are results computed with conventional DFT (black) and DFT-D3 (red) as well as images of the initial, transition, and final states.

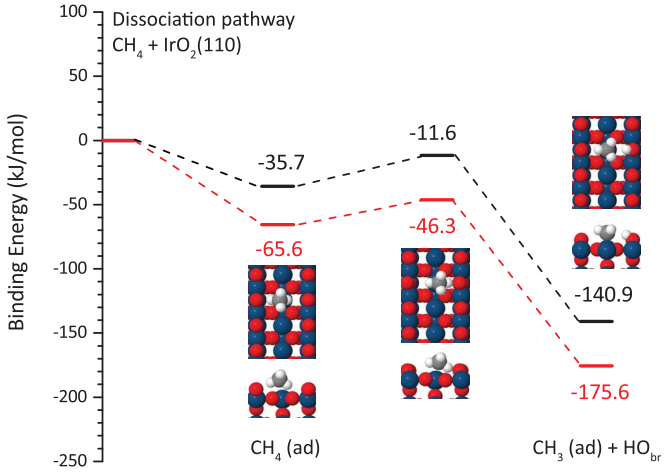

the DFT calculations can be found in the supplementary materials along with CH_4 adsorption energies obtained by using several DFT functionals that incorporate dispersion. The calculations predict a facile pathway for C–H bond cleavage of CH_4 on IrO_2(110). A plot of the charge-density difference (fig. S4) shows that the CH_4 molecule forms a strongly bound σ complex on IrO_2(110) by adopting an η^2 configuration and datively bonding with a single Ir_{cus} atom. Back donation of charge from the Ir_{cus} atom to CH_4 weakens the C–H bond and promotes C–H bond cleavage. In the C–H bond cleavage step, the CH_4 complex transfers an H atom to a neighboring O_{br} atom, resulting in CH_3-Ir_{cus} and HO_{br} moieties. Both the DFT and DFT-D3 calculations predict that the energy barrier for dissociation lies below the gas-phase energy level so that C–H bond cleavage is energetically preferred over desorption of the adsorbed CH_4 complex.

The dispersion correction included in the DFT-D3 calculations increased the binding energies computed for each adsorbed state compared with the results of the DFT-PBE calculations. Because the enhancement is similar for the initial state and the transition state, both the DFT and DFT-D3 calculations predict similar values for the C–H bond cleavage barrier relative to the initial adsorbed state (E_r ~ 24 versus 19 kJ/mol), where these values agreed reasonably well with the value of E_r = 28.5 kJ/mol estimated from our experimental data. Also, our experimental estimates of the binding energy and apparent dissociation barrier for the adsorbed CH_4 complex agreed well with the values computed by using DFT-PBE. From our experimental data, we estimate values of E_d ~ 38 kJ/mol and $E_r - E_d$ = −9.5 kJ/mol, where these values agree to within better than 2.5 kJ/mol of the values predicted by DFT-PBE (E_d = 35.7 kJ/mol; $E_r - E_d$ = −11.6 kJ/mol). The rate coefficient governing the recombinative desorption of CH_4 via the reaction $CH_3 + HO_{br} \rightarrow CH_4(g) + O_{br}$ is approximately equal to the rate coefficient for only the recombination step that produces the adsorbed CH_4 σ complex when the temperature is sufficiently high. The results of both our DFT-PBE and DFT-D3 calculations predict an energy barrier of about 129 kJ/mol for this recombination step (Fig. 4). For desorption prefactors of 10^{12} and 10^{13} s^{-1}, we estimate that the CH_4 TPRS peak observed at 515 K corresponds to activation energies of 130 and 140 kJ/mol, respectively.

The facile activation of CH_4 on cus-Ir-O surface pairs may provide opportunities for developing catalysts and catalytic processes that can promote efficient and selective methane functionalization. For example, certain coreactants may directly react with CH_4-derived fragments on IrO_2(110) to produce value-added compounds. It may also be possible to modify the IrO_2(110) surface to limit its oxidizing power and/or incorporate cus-Ir-O surface pairs into other materials that promote more desirable methane chemistries, such as conversion to organic oxygenates or higher hydrocarbons.

REFERENCES AND NOTES

1. R. Horn, R. Schlogl, *Catal. Lett.* **145**, 23–39 (2015).
2. W. Taifan, J. Baltrusaitis, *Appl. Catal. B* **198**, 525–547 (2016).
3. J. F. Weaver, A. F. Carlsson, R. J. Madix, *Surf. Sci. Rep.* **50**, 107–199 (2003).
4. T. S. Wittrig, P. D. Szuromi, W. H. Weinberg, *J. Chem. Phys.* **76**, 3305–3315 (1982).
5. P. D. Szuromi, J. R. Engstrom, W. H. Weinberg, *J. Phys. Chem.* **89**, 2497–2502 (1985).
6. C. B. Mullins, W. H. Weinberg, *J. Chem. Phys.* **92**, 4508–4512 (1990).
7. A. V. Hamza, H. P. Steinruck, R. J. Madix, *J. Chem. Phys.* **86**, 6506–6514 (1987).
8. C. T. Campbell, J. R. V. Sellers, *Chem. Rev.* **113**, 4106–4135 (2013).
9. E. W. McFarland, H. Metiu, *Chem. Rev.* **113**, 4391–4427 (2013).
10. L. Chen, R. S. Smith, B. D. Kay, Z. Dohnalek, *Surf. Sci.* **650**, 83–92 (2016).
11. J. F. Weaver, C. Hakanoglu, A. Antony, A. Asthagiri, *Chem. Soc. Rev.* **43**, 7536–7547 (2014).
12. J. F. Weaver, *Chem. Rev.* **113**, 4164–4215 (2013).
13. F. Zhang *et al.*, *Angew. Chem. Int. Ed.* **54**, 13907–13911 (2015).
14. C. Hall, R. N. Perutz, *Chem. Rev.* **96**, 3125–3146 (1996).
15. N. M. Martin *et al.*, *ACS Catal.* **4**, 3330–3334 (2014).
16. C. C. Wang, S. S. Siao, J. C. Jiang, *J. Phys. Chem. C* **116**, 6367–6370 (2012).
17. A. Antony, thesis, University of Florida, Gainesville, FL (2013).
18. T. L. M. Pham, E. G. Leggesse, J. C. Jiang, *Catal. Sci. Technol.* **5**, 4064–4071 (2015).

19. T. Li *et al.*, *Phys. Chem. Chem. Phys.* **18**, 22647–22660 (2016).
20. T. Li *et al.*, *J. Phys. Chem. C* **120**, 9863–9873 (2016).
21. B. A. Arndtsen, R. G. Bergman, *Science* **270**, 1970–1973 (1995).
22. C. T. Reeves, D. C. Seets, C. B. Mullins, *J. Mol. Catal. Chem.* **167**, 207–215 (2001).
23. Y. B. He *et al.*, *J. Phys. Chem. C* **112**, 11946–11953 (2008).
24. W. H. Chung, D. S. Tsai, L. J. Fan, Y. W. Yang, Y. S. Huang, *Surf. Sci.* **606**, 1965–1971 (2012).
25. R. Rai *et al.*, *Surf. Sci.* **652**, 213–221 (2016).
26. C. T. Rettner, E. K. Schweizer, H. Stein, D. J. Auerbach, *Phys. Rev. Lett.* **61**, 986–989 (1988).
27. S. Grimme, J. Antony, S. Ehrlich, H. Krieg, *J. Chem. Phys.* **132**, 154104 (2010).

ACKNOWLEDGMENTS

We acknowledge financial support for this work provided by SABIC. We also acknowledge the Ohio Supercomputing Center for providing computational resources. All results are reported in the main paper and supplementary materials.

SUPPLEMENTARY MATERIALS

www.sciencemag.org/content/356/6335/299/suppl/DC1
Materials and Methods
Supplementary Text
Figs. S1 to S4
Table S1
References (*28–41*)

3 February 2017; accepted 24 March 2017
10.1126/science.aam9147

Science
AAAS

Low-temperature activation of methane on the IrO_2(110) surface

Zhu Liang, Tao Li, Minkyu Kim, Aravind Asthagiri and Jason F. Weaver (April 20, 2017)

Science **356** (6335), 299-303. [doi: 10.1126/science.aam9147]

Editor's Summary

Low-temperature methane reactions

Methane is a potential feedstock for more valuable products. The strong carbon-hydrogen bonds of methane can be activated by heterogeneous catalysts but often at temperatures that make it difficult to control reactions selectively. Liang *et al.* show that methane, adsorbed on the stoichiometric IrO_2 (110) under ultrahigh-vacuum conditions, reacts with exposed iridium atoms to break the carbon-hydrogen bonds at temperatures as low as 150 K. On heating, the surface fragments react cleanly with surface oxygen to form carbon dioxide, carbon monoxide, and water.

Science, this issue p. 299

Science (print ISSN 0036-8075; online ISSN 1095-9203) is published weekly, except the last week in December, by the American Association for the Advancement of Science, 1200 New York Avenue NW, Washington, DC 20005.